ACS APPLIED MATERIALS & INTERFACES

Research Article

www.acsami.org

A Highly Sensitive Hydrogen Sensor with Gas Selectivity Using a PMMA Membrane-Coated Pd Nanoparticle/Single-Layer Graphene Hybrid

Juree Hong,[†] Sanggeun Lee,[†] Jungmok Seo,[†] Soonjae Pyo,[‡] Jongbaeg Kim,[‡] and Taeyoon Lee*[,†]

[†]Nanobio Device Laboratory, School of Electrical and Electronic Engineering, and [‡]Nano Tranducers Laboratory, School of Mechanical Engineering, Yonsei University, 50 Yonsei-Ro, Seodaemun-Gu, Seoul 120-749, Republic of Korea

Supporting Information

ABSTRACT: A polymer membrane-coated palladium (Pd) nanoparticle (NP)/single-layer graphene (SLG) hybrid sensor was fabricated for highly sensitive hydrogen gas (H_2) sensing with gas selectivity. Pd NPs were deposited on SLG via the galvanic displacement reaction between graphene-buffered copper (Cu) and Pd ion. During the galvanic displacement reaction, graphene was used as a buffer layer, which transports electrons from Cu for Pd to nucleate on the SLG surface. The deposited Pd NPs on the SLG surface were well-distributed with high uniformity and low defects. The Pd NP/SLG hybrid was then coated with polymer membrane layer for the selective filtration of H_2. Because of the selective H_2 filtration effect of the polymer membrane layer, the sensor had no responses to methane, carbon monoxide, or nitrogen dioxide gas. On the contrary, the PMMA/Pd NP/SLG hybrid sensor exhibited a good response to exposure to 2% H_2: on average, 66.37% response within 1.81 min and recovery within 5.52 min. In addition, reliable and repeatable sensing behaviors were obtained when the sensor was exposed to different H_2 concentrations ranging from 0.025 to 2%.

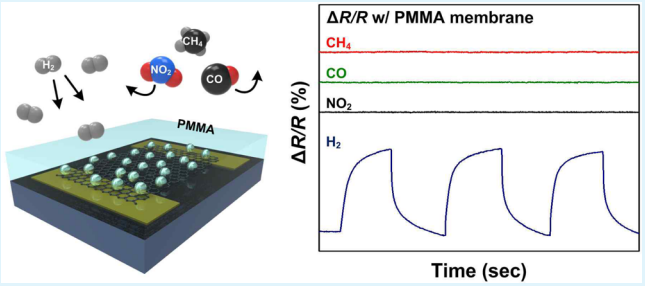

KEYWORDS: *PMMA membrane, selective hydrogen sensor, Pd nanoparticle/graphene hybrid, galvanic displacement reaction*

1. INTRODUCTION

Hydrogen gas (H_2) is one of the cleanest and the most promising energy sources, and because of its energy density, renewability, and ecofriendly nature, it has the potential to serve as an emissions-free alternative fuel.[1−4] However, the use of H_2 as an alternative energy source is associated with several safety issues requiring accurate and fast leakage detection, namely, the low spark ignition energy (0.02 mJ) and wide flammable range (4−75%) of H_2.[4−6] Several types of H_2 sensors have been developed, including metal-oxide based sensors, thin film metal based sensors, and acoustic wave based sensors.[7−12] Among these H_2 sensors, most commercially available H_2 sensors are based on metal oxides (e.g., In_2O_3, SnO_2, ZnO, and TiO_2) because of their simple structures and decent gas sensing properties.[13−16] However, these metal oxide-based H_2 sensors usually require high temperatures over 400 °C to maintain operation with optimal sensitivity, which is a significant drawback.[17,18] To lower the optimal operation temperature, metal oxide-based H_2 sensors have been decorated with noble metal catalysts, such as gold (Au), platinum (Pt), ruthenium (Ru), and palladium (Pd) because of their superior hydrogen solubility at room temperature.[7,19−24] Although noble metal-decorated metal oxide-based H_2 sensors are capable of the low temperature operation with improved sensitivity upon exposure to H_2, they suffer from cross-sensitivity issues with carbon monoxide gas (CO) and hydrocarbon gases including methane gas (CH_4) arising from the presence of a noble metal catalyst.[25,26]

Recently, graphene has attracted significant interest as a chemical sensing material because of its unique structural, mechanical, and electrical properties.[27−30] Because graphene has a maximum surface area with respect to its volume that is due to a perfect two-dimensional structure with just one layer of carbon atoms, graphene-based sensors can provide a large gas adsorptive capacity.[31] Moreover, graphene-based sensors can effectively detect polar molecules, such as CO, nitrogen dioxide (NO_2), and ammonia gas because the electrical conductivity of graphene changes drastically upon exposure to these gases with low noise level due to its chemically inert properties and high carrier mobility at room temperature.[27,28] However, in spite of the excellent gas-sensing properties of graphene toward various polar molecules, it is insensitive to most nonpolar molecules including H_2.[28] Therefore, graphene-based H_2 sensors require noble metal catalysis to effectively detect H_2, similar to metal oxide-based H_2 sensors decorated with noble metal catalysts such as Au, Pt and Pd. Importantly,

Received: October 23, 2014
Accepted: January 29, 2015
Published: January 29, 2015

DOI: 10.1021/am5073645
ACS Appl. Mater. Interfaces 2015, 7, 3554−3561

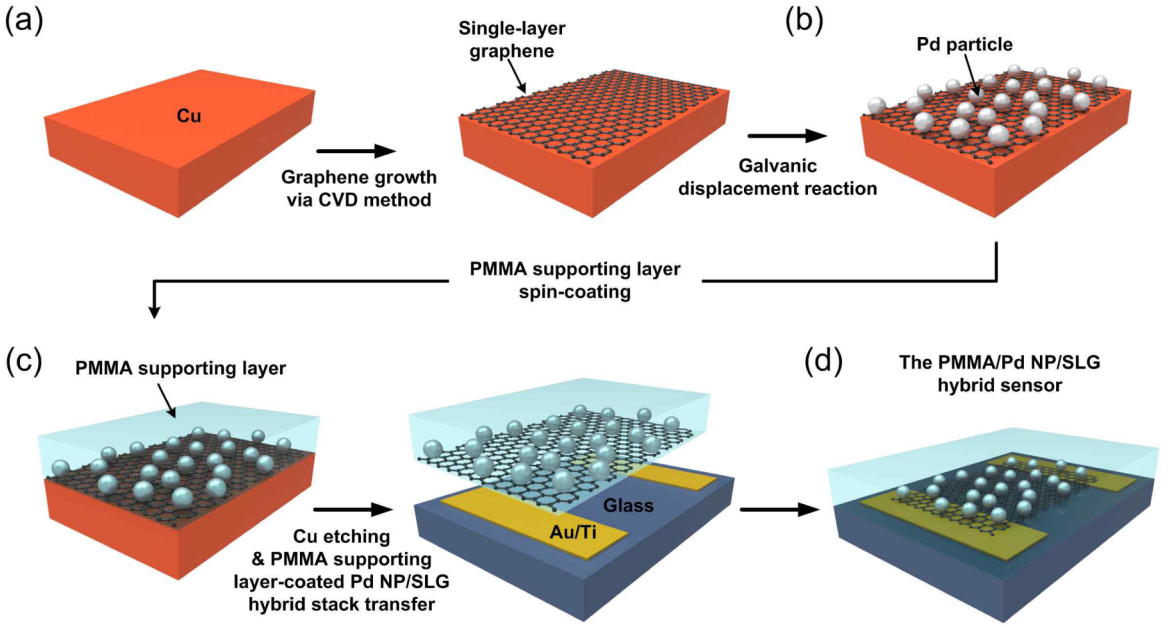

Figure 1. Schematic illustration of the procedures used to fabricate the PMMA/Pd NP/SLG hybrid sensor. Illustration of (a) the growth of SLG on Cu foil, (b) the Pd NPs deposited on SLG via galvanic displacement reaction, (c) the transfer of Pd NP/SLG hybrid onto the electrode-patterned glass substrate, and (d) the fabrication of the PMMA/Pd NP/SLG hybrid sensor.

several studies have reported that noble metal-decorated graphene-based H_2 sensors exhibit high sensitivity as well as fast response and recovery for H_2 sensing at room temperature.[32−35] Nevertheless, despite the high sensing performance of noble metal-decorated graphene-based H_2 sensors at room temperature, cross sensitivity with CO, CH_4, and NO_2 remains a critical issue. Because H_2 sensors should be able to survive multiple exposures to H_2 without damage, a highly sensitive H_2 sensor with good gas selectivity is desirable for sensor operation in the context of contaminated environments.

In this report, we fabricated polymer membrane-coated Pd nanoparticle (Pd NP)/single-layer graphene (SLG) hybrids for highly sensitive H_2 sensing with gas selectivity. SLG was grown on copper (Cu) foil via a chemical vapor deposition (CVD) method and Pd NPs were deposited on SLG/Cu foil via a graphene-buffered galvanic displacement reaction between Cu and Pd ions. Poly(methyl methacrylate) (PMMA) was spin-coated on Pd NP/SLG hybrids as a polymer membrane for selective filtration of H_2. The fabricated PMMA membrane-coated Pd NP/SLG (PMMA/Pd NP/SLG) hybrid sensor exhibited high gas response sensitivity of 66.67% within 1.81 min on average upon exposure to 2% H_2 at room temperature. Sensor recovery to its initial state was achieved within 5.52 min on overage after completely turning off the H_2 source and purging the chamber with air at room temperature, which indicates that our PMMA/Pd NP/SLG hybrid sensor had a highly reliable performance toward H_2 detection. On the contrary, the fabricated PMMA/Pd NP/SLG hybrid sensor did not response upon exposure to other gases (CH_4, CO, and NO_2), indicating a highly selective performance toward H_2. Specifically, the PMMA membrane layer on the top of the Pd NP/SLG hybrid sensor acted as a selective filtration layer because of the moderate free volume of the PMMA polymer matrix that only allowed H_2 to penetrate. Taken together, the results of the present study indicate that the PMMA/Pd NP/SLG hybrid sensor was highly sensitive toward H_2 without interference from other gases in the presence of contaminated backgrounds.

2. EXPERIMENTAL SECTION

2.1. Fabrication Procedures. Figure 1 schematically illustrates the fabrication procedures of the PMMA/Pd NP/SLG hybrid sensor on the glass substrate. The procedure involved four main steps: growth of SLG on Cu foil, deposition of Pd NPs on SLG, transfer of Pd NP/SLG hybrid onto the electrode-patterned glass substrate, and fabrication of the PMMA/Pd NP/SLG hybrid sensor. The SLG was grown using a CVD method on catalytic Cu foil.[36,37] Next, the SLG layer on the backside of the Cu foil was removed by oxygen plasma etching to expose one side of Cu. This SLG/Cu backside etching process was essential for the next step: deposition of Pd NPs on SLG via a galvanic displacement reaction. In the absence of the etching process of SLG on the backside of the Cu foil, a galvanic displacement reaction between Cu and Pd ions cannot occur due to the remaining SLG grown on the backside of Cu. Pd NP deposition on top of the SLG layer was achieved by immersing the SLG/Cu sample in a solution of $PdCl_2$ to facilitate a galvanic displacement reaction. The density of Pd NPs on SLG could be tailored by controlling the concentration of the $PdCl_2$ solution as well as immersion time. After Pd NP deposition, the Pd NP/SLG hybrid sample was spin-coated with a polymer-supporting layer and floated on an etchant solution for Cu etching process. After complete Cu etching, the polymer-supporting layer-coated Pd NP/SLG hybrid stack was manually laid onto the electrode-patterned glass substrate. Finally, the PMMA layer was spin-coated once again to generate a gapless PMMA membrane layer.

2.2. Growth of Single-Layer Graphene. For the growth of single-layer graphene (SLG), a 70-μm-thick Cu foil (Wacopa, purity 99.9%) was cut into 2 × 2 cm^2 pieces and loaded into a quartz tube furnace. Cu foil samples were first annealed by heating to 1077 °C under a H_2 flow (50 sccm) for 30 min at atmospheric pressure, and then the SLG was formed by adjusting the chamber pressure to 2 Torr under a continuous flow of H_2 and CH_4 (10 sccm) at 1000 °C for 60 min.

2.3. Preparation of the Pd NP/Graphene Hybrid. The backside graphene of the Cu foil was removed using O_2 plasma etching (100 W, 90 s) prior to Pd NP deposition. The as-obtained SLG/Cu foil sample

DOI: 10.1021/am5073645
ACS Appl. Mater. Interfaces 2015, 7, 3554−3561

was then immersed in an aqueous palladium chloride ($PdCl_2$) solution containing 0.01 g $PdCl_2$ and 0.1 g NaCl in 300 mL DI water for 1 to 120 min for Pd NP deposition. The deposition of Pd NP on graphene was based on a galvanic displacement reaction between Pd ions and Cu under graphene. After the galvanic displacement reaction, SLG/Cu foil samples were rinsed with DI water, dried with N_2 blowing, and baked on hot plate at 100 °C for 10 min to evaporate any remaining water molecules.

2.4. Fabrication of PMMA Membrane-Coated a Pd NP/SLG Hybrid Sensor. A 50/10 nm-thick Au/Ti electrode was deposited on the glass substrate via a thermal evaporation system by using a shadow mask with a line width of 1 mm. To transfer the as-prepared Pd NP/SLG hybrid onto the electrode-patterned glass substrate, a 200 nm-thick PMMA supporting layer (Sigma-Aldrich; average molar weight ~996,000, dissolved in anisole to a concentration of 40 mg mL^{-1}) was spin-coated on the as-prepared Pd NP/SLG hybrid/Cu foil at 4000 rpm for 30 s. To etch the Cu foil, the polymer supporting layer-coated Pd NP/SLG/Cu stack was floated on a 0.1 M ammonium persulfate solution. After etching of the Cu foil, the floating polymer supporting layer-coated Pd NP/SLG hybrid stack was moved to a 5:1:1 solution of H_2O−H_2O_2−HCl and kept for 15 min in a floating state to remove any remaining etchant residue. Then, the polymer supporting layer-coated Pd NP/SLG hybrid stack was floated on DI water and rinsed to remove the remaining residue. The floating PMMA supporting layer-coated Pd NP/SLG hybrid stack was then manually transferred to a glass substrate with predefined electrodes, followed by baking on a hot plate at 60 °C for 30 min. To make the 400-, 600-, and 800 nm-thick PMMA membrane layers, the 200 nm-thick PMMA/Pd NP/SLG hybrid sensor was successively spin-coated again with a PMMA solution at 4000 rpm for 30 s. A 400 nm-thick PMMA membrane-coated Pd NP/SLG hybrid sensor was expressed as a PMMA/Pd NP/SLG hybrid sensor in this experiment. In the case of using other PMMA layer thicknesses, we mentioned the thickness of PMMA. To prepare a sensor without PMMA, the final sensor was immersed into an acetone solution for 30 min to remove the PMMA supporting layer.

2.5. Gas Sensing Measurement. For gas sensing, the PMMA/Pd NP/SLG hybrid sensor was first placed into a quartz tube furnace. The sensor was then exposed to air (500 sccm) for 5 min to allow for initialization, and then H_2 or other gases (CH_4, CO, and NO_2) diluted in N_2 was introduced to measure the change in resistance response. To evaluate recovery of the sensor, air was injected into the tube furnace. The resistance changes were measured using a Keithley 2400 source measurement unit connected to two electrical wires using a feedthrough. The bias voltage was fixed at 10 mV.

2.6. Characterization. The thickness of PMMA layer was confirmed by an alpha-step 500 surface profiler (Tencor Instruments). The morphology and elemental composition of Pd NP on SLG was examined using a JEOL JSM-7001F field emission scanning electron microscope (FE-SEM). The elemental confirmation of Pd NPs on SLG after the galvanic displacement reaction was investigated with the FE-SEM-EDS link system (JEOL, 3000F). As-grown SLG and Pd NP/SLG hybrid were confirmed using a Jobin-Yvon micro-Raman system (LabRam HR, 532 nm wavelength, 5 mW power, and 1-μm spot size).

3. RESULTS AND DISCUSSION

Figure 2a shows a schematic illustration of the Pd deposition process on CVD-grown SLG via the galvanic displacement reaction process using Cu as the reducing agent. Since the standard electrochemical potential of Cu (0.34 V) is lower than that of Pd (0.915 V), the metal exchange process between Cu and Pd ions could be successfully performed by simply immersing Cu in a Pd-ion-containing salt solution. Specifically, as Cu was immersed in the Pd-ion-containing salt solution, Cu was oxidized by Pd and provide electrons for Pd ions to be simultaneously reduced and nucleated on the Cu surface.[38,39] In this metal exchange process, a direct galvanic replacement occurred between Cu and Pd^{2+} on bare Cu surfaces, and thus the resulting Pd NPs formed irregular shapes as they filled out

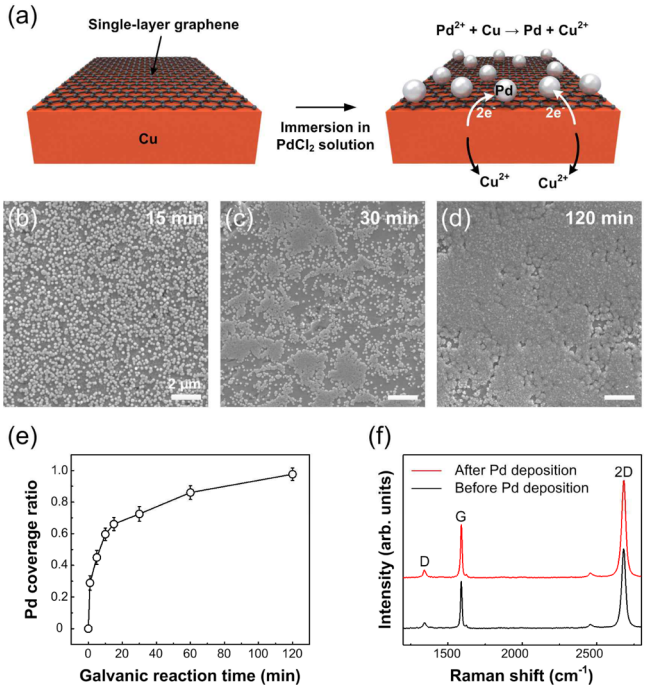

Figure 2. (a) Schematic of the Pd NP deposition process on CVD-grown graphene via galvanic displacement reaction. (b–d) FE-SEM micrographs of Pd NPs/SLG/Cu samples after galvanic displacement reaction for (b) 15, (c) 30, and (d) 120 min. Scale bars indicate 2 μm. (e) Changes in the surface coverage, c_{pd}, of Pd on graphene for various galvanic displacement reaction times. (f) Micro-Raman spectra before Pd deposition (black solid line) and after Pd deposition (red solid line).

the empty space on Cu. In the presence of the graphene layer above Cu, graphene acted as a buffer layer to transport electrons from Cu onto the graphene surface due to its high carrier mobility and conductivity. In this case, Pd NPs nucleated on the graphene surface by obtaining electrons from graphene. Since the galvanic displacement reaction was buffered with the graphene layer, the Pd nucleation on graphene was not limited to a specific region of the graphene surface and the resulting Pd NPs were well-distributed spatially on the SLG surface, unlike galvanic displacement on a bare Cu surface. Figure 2b–d are representative of the top-view FE-SEM images of the Pd NPs deposited on graphene layers as a function of immersion time in the same concentration of $PdCl_2$ solution (0.18 mM). Specifically, the Pd NPs on the graphene surface were uniformly distributed with spherical shapes along the graphene. The Pd NPs on the graphene surface were confirmed by conducting the FE-SEM-EDS mapping analysis as shown in Figure S1 in the Supporting Information. When immersion time was less than 15 min, Pd NPs were distributed separately on the SLG surface with an average diameter of 20 nm (Figure 2b), while Pd NPs began to form islands after being immersed for more than 15 min in the $PdCl_2$ solution (Figure 2c). At an immersion time of 120 min, the surface coverage (c_{pd}) of Pd on SLG nearly reached 1, resulting in a Pd film-like structure on the SLG surface (Figure 2d). Figure 2e shows the changes in c_{pd} with varying immersion time from 1 to 120 min: increasing immersion time led to a gradual increase in c_{pd} from 0.28 to 0.97. To more closely examine the damage on graphene that could be generated during the galvanic displacement reaction between graphene-buffered Cu and Pd ions, wer took

DOI: 10.1021/am5073645
ACS Appl. Mater. Interfaces 2015, 7, 3554–3561

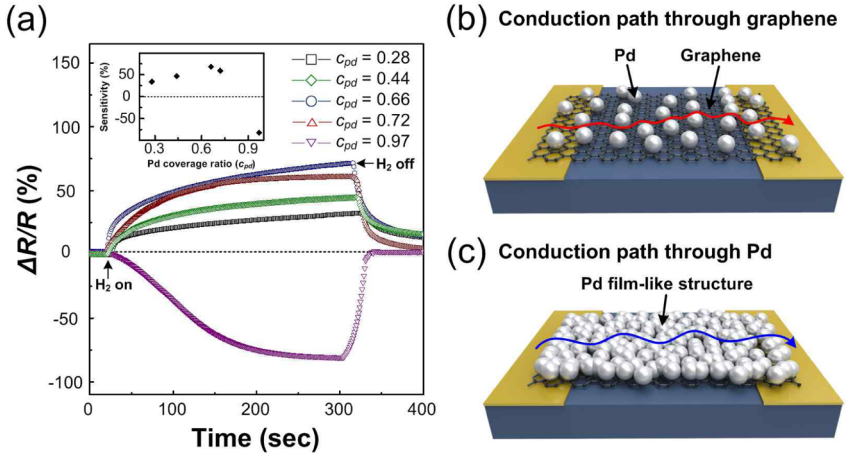

Figure 3. (a) Relative resistance response (shown as a percent) of PMMA/Pd NP/SLG hybrid sensors with different value of c_{pd} on SLG as a function of time when exposed to 2% H_2. The inset shows a plot of sensitivity versus c_{pd} on SLG layer. (b, c) Schematic representation of the conduction path through (b) graphene and (c) Pd.

micro-Raman spectra from graphene samples before and after the 15 min galvanic displacement reaction, as shown in Figure 2f. The ratio of the intensities of the G peak to the 2D peak (I_G/I_{2D}) of our CVD-grown graphene was 0.49, whereas a minor D peak intensity (I_D) was observed near 1350 cm^{-1}; these results indicated that our CVD-grown graphene was indeed a SLG with few structural defects.[40] Importantly, the I_G/I_{2D} ratio and the I_D in micro-Raman spectra were nearly identical after the galvanic displacement reaction, indicating that there was almost no damage to the intrinsic graphene structure. If there are intrinsically destroyed regions on graphene surface, such as cracks, voids, and ripped parts, the galvanic displacement reaction will take place preferentially on those sites due to the presence of the exposed Cu. In such cases, neighboring graphene could be damaged during the galvanic displacement reaction because of rapid and concentrative deposition of Pd on the destroyed regions. Because the fabricated SLG had almost no intrinsic cracks, voids, and ripped parts, damages on SLG were not found after the galvanic displacement reaction. The result in Figure 2f indicates that the graphene layer effectively acted as a buffer layer, retaining its structure even after undergoing a galvanic displacement reaction in Pd-ion containing salt solution.

To examine the gas response of PMMA/Pd NP/SLG hybrid sensors with respect to Pd NP coverage on the SLG layer, we plotted the percent change in relative resistance as a function of time after exposure of PMMA/Pd NP/SLG hybrid sensors to 2% H_2. The relative resistance value change was defined as $\Delta R/R = (R_{exposure} - R_{initial})/R_{initial}\cdot 100$, where $R_{initial}$ and $R_{exposure}$ were the resistances of the sensors before and after exposure to H_2, respectively. For measuring $\Delta R/R$, a fixed bias of 10 mV was applied. Figure 3a shows the changes in resistance across the electrodes of the PMMA/Pd NP/SLG hybrid sensors with different degrees of Pd NP coverage. The inset of Figure 3a shows a plot of the gas response sensitivity versus Pd NP coverage on the SLG layer. As the Pd NP coverage on the SLG layer increased, the value of $\Delta R/R$ gradually increased upon H_2 exposure, exhibiting the highest sensitivity (65%) with c_{pd} = 0.66. The gradual increase of the gas response sensitivity was attributed to the increased coverage of Pd NPs on the SLG surface.[34] However, the gas response sensitivity of the PMMA/Pd NP/SLG hybrid sensor with c_{pd} = 0.72 was measured to be 58%, which was slightly lower than that of the PMMA/Pd NP/SLG hybrid sensor with c_{pd} = 0.66. In addition, the PMMA/Pd NP/SLG hybrid sensor with c_{pd} = 0.97 went so far as to exhibit adverse behavior in resistance changes, showing a huge decrease in $\Delta R/R$ upon H_2 exposure with a percent change in gas response sensitivity of −82%. All sensors in Figure 3a showed complete recovery to the initial baseline within a few minutes after H_2 was shut off. The two different behaviors, which were determined as positive and negative signs of $\Delta R/R$ depending on Pd NP coverage on SLG, were attributed to different electrical conduction paths of the sensors, namely, a graphene-dominant conduction path for low Pd NP coverage on SLG and Pd film-dominant conduction path for high Pd NP coverage on SLG. When Pd NPs were distributed separately on the SLG surface with a low c_{pd} below 0.66, the graphene served as the major conduction path, as shown in Figure 3b. In this case, $\Delta R/R$ was a positive value because resistance increased upon H_2 exposure. On the other hand, a negative $\Delta R/R$ was observed when Pd NPs formed a uniform Pd film-like structure on the SLG surface with a high c_{pd} over 0.72 as shown in Figure 3c, indicating that Pd filmlike structure was the major conduction path upon H_2 exposure. The mechanism of H_2 detection of sensors with a graphene-dominant conduction path can be explained by the well-known dissolution and dissociation of H_2 molecules into atomic hydrogen in Pd NPs.[32] When H_2 molecules are adsorbed on Pd NP surfaces and dissolved into atomic hydrogen, Pd-hydride (PdH_x) is formed as the work function of Pd is lowered. The lower work function associated with PdH_x results in increased electron transfer to graphene from PdH_x, which in turn increases sensor resistance. As the density of Pd NPs increases on the SLG surface, the probability of forming PdH_x also increases due to the increased high surface area of Pd. However, the gas response sensitivity decreases when the Pd NPs begin to form islands on the SLG surface, because the major conduction path starts to change from graphene to a Pd film-like structure. When the coverage of Pd NPs approaches ∼1 on an SLG, the Pd film-like structure becomes the main conduction path of the sensor. In this case, the sensing mechanism is based on the hydrogen-induced lattice expansion in Pd. When Pd becomes PdH_x upon exposure to H_2, the Pd layer is expanded because of the filling of octahedral sites of the Pd system by H atoms.[41,42] The volumetric expansion of the Pd NPs on SLG can narrow the gaps between Pd NPs in Pd film-like structure on SLG.

DOI: 10.1021/am5073645
ACS Appl. Mater. Interfaces 2015, 7, 3554−3561

Therefore, Pd filmlike structures become continuous, more conductive pathways are formed,[34,43] and resistance decreases upon H_2 exposure. We confirmed that the absolute value of the sensitivity of the PMMA/Pd NP/SLG hybrid sensor with c_{pd} = 0.97 was 82%, which was the highest gas response sensitivity among our fabricated sensors. However, in spite of this high gas response sensitivity, maintaining sensor reliability was problematic. The PMMA/Pd NP/SLG hybrid sensor with c_{pd} = 0.97 exhibited unstable gas response properties due to hydrogen-induced expansion-contraction and associated crack propagation during a repeated sensing process (data not shown). The PMMA/Pd NP/SLG hybrid sensor with a low c_{pd} under 0.72 showed a stable gas response with high sensitivity after repeated tests.

To evaluate the sensing performance of the PMMA/Pd NP/SLG hybrid sensor upon exposure to H_2, 10 sensors were fabricated by using the optimized condition (c_{pd} = 0.66). Figure S2 in the Supporting Information represents the percent changes in relative resistance as a function of time after exposure of the 10 sensors to 2% H_2. The average values of gas response sensitivity, response time, and recovery time was measured as 66.37%, 1.81 min, and 5.52 min, respectively. The sample-to-sample variation between individual sensors in Figure S2 would be inevitably caused during the sensor fabrication process, which includes solution-based galvanic reaction, polymer layer coating, and transfer process. Among these sensors, a PMMA/Pd NP/SLG hybrid sensor, which had near average sensitivity, response time, and recovery time, was selected for the evaluation of sensing performance. Figure 4a shows the reproducible resistance change of the selected PMMA/Pd NP/SLG hybrid sensor with c_{pd} = 0.66. To evaluate repeatability, ~5 min on-state and ~20 min off-state were performed with 2% H_2. The gas response sensitivity was as high as 66.38% for each cycle. The response time, defined as the rise time needed to reach a ΔR of 90%, was about 1.07 min and the resistance recovered to its original value within 11.28 min without any significant drift when H_2 was removed and the test chamber was purged with air. The PMMA/Pd NP/SLG hybrid sensor had good repeatability and reversibility, demonstrating relatively fast and stable on/off switching in each cycle. Figure 4b shows the in situ measurement of the resistance change in percent when exposed to different concentration of H_2 ranging from 0.025 to 2% (the specific concentrations are labeled above each peak in Figure 4b). Prior to exposure to H_2, only air flowed in test chamber, followed by exposure to H_2 for 5 min. Then, H_2 was shut off and only air flowed into the test chamber for 10 min to allow the sensor to recover. The gas response sensitivity as a function of H_2 concentration was roughly linear on a logarithmic scale as shown in the inset of Figure 4b. As the concentration of H_2 increased, the gas response sensitivity also increased, and the sensor exhibited an observable resistance change (an approximately 4.014% change in gas response sensitivity) with a low noise level at concentrations as low as 250 ppm. On the basis of these results, we concluded that the sensing performance of the PMMA/Pd NP/SLG hybrid sensor was comparable or superior to other reported hydrogen sensors based on graphene-Pd hybrids.[32−35]

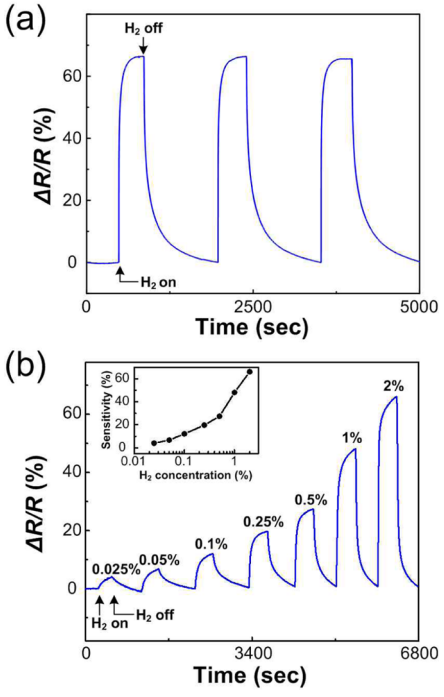

Figure 4. Evaluation of sensing performance of the PMMA/Pd NP/SLG hybrid sensor with c_{pd} = 0.66 as a function of time (a) Reproducible resistance changes upon exposure to 2% H_2. (b) In situ measurement of percent change in resistance upon exposure to different concentrations of H_2 ranging from 0.025 to 2%. The inset shows a plot of gas response sensitivity with respect to H_2 concentration on a log scale.

To evaluate the selective gas permeation property of PMMA in our fabricated sensors, the gas response of Pd NP/SLG hybrid sensor both with and without the PMMA membrane layer was investigated for different types of gases (CH_4, CO, NO_2, and H_2). These four different gases were chosen because they are known to react with either Pd, graphene, or in some cases both. Indeed, graphene exhibits cross-sensitivity toward both CO and NO_2,[28] whereas Pd reacts with CO and hydrocarbon gases including CH_4.[25,26,44] Figure 5a depicts schematic illustrations of possible routes of selective permeation of H_2 in the presence of a PMMA membrane layer as well as cross sensitivity toward various gases in the absence of the PMMA membrane layer. Prior to the evaluation of the H_2 selective permeation property of the PMMA membrane-coated sensors, the optimal thickness of the PMMA layer was investigated by comparing the values of the gas response sensitivities depending on the PMMA membrane thicknesses (200, 400, 600, and 800 nm). To avoid the sample-to-sample variation, the gas response sensitivity of the same Pd NP/SLG hybrid sensor was successively evaluated after additional repeating of the PMMA spin-coating on top of the sensor. A 200 nm thick PMMA layer, which was initially coated as a supporting layer for the transfer of the Pd NP/SLG hybrid sensor, did not function as a selectively H_2-permeable membrane due to imperfect sealing of the sensor because the 200 nm thick PMMA layer only holds the Pd NP/SLG hybrid region without covering the whole sensor. The 200 nm-thick PMMA/Pd NP/SLG hybrid sensor reacted with 2% CO (~10% in gas response sensitivity) as well as 2% H_2 (approximately 100% in gas response sensitivity) as shown in Figure S3 in the Supporting Information. When the PMMA thickness increased from 400 to 800 nm, the gas response sensitivity upon exposure to 2% H_2 decreased from ~65% to 26% as shown in Figure S3a in the Supporting Information. This results is coincident with the fact that the permeability decreases with increased polymer membrane thickness due to a

DOI: 10.1021/am5073645
ACS Appl. Mater. Interfaces 2015, 7, 3554−3561

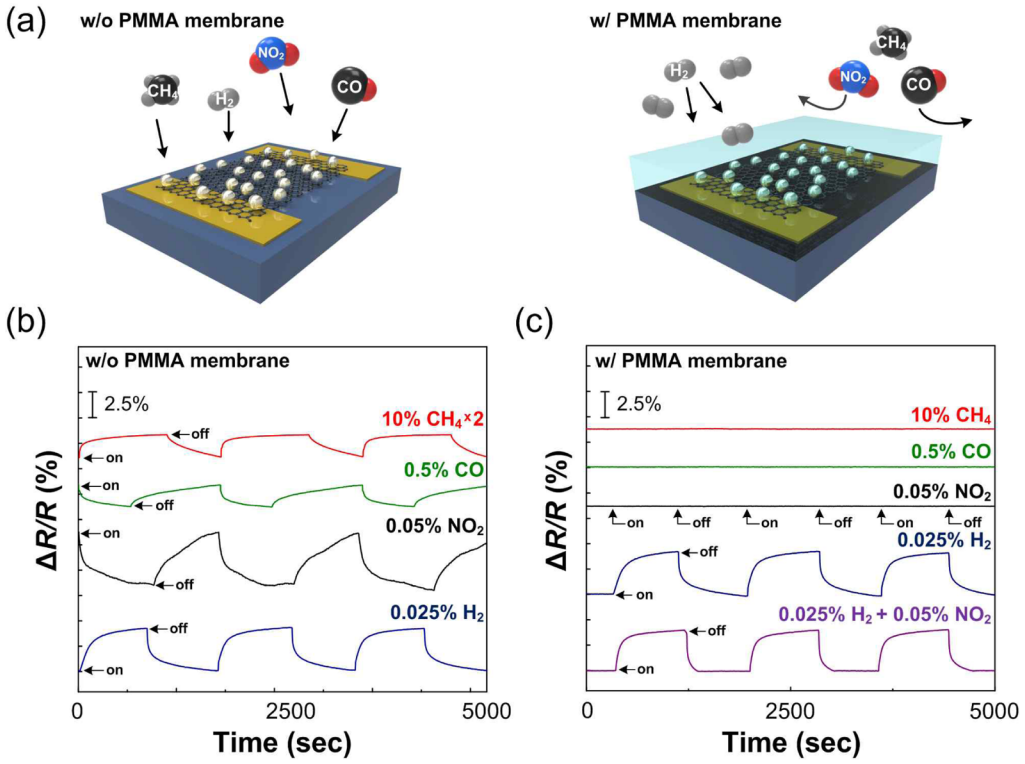

Figure 5. (a) Schematic illustration showing the selective permeation of H_2 through the PMMA membrane layer and reaction with all gases without the PMMA layer. (b) Relative resistance changes of the Pd NP/SLG hybrid sensor for different gases: 10% CH_4 (red solid line), 0.5% CO (green solid line), 0.05% NO_2 (black solid line), and 0.025% H_2 (blue solid line) (c) Relative resistance changes of the PMMA/Pd NP/SLG hybrid sensor when exposed to10% CH_4 (red solid line), 0.5% CO (green solid line), 0.05% NO_2 (black solid line), 0.025% H_2 (blue solid line), and mixture gases of 0.025% H_2 and 0.05% NO_2 (purple solid line), respectively.

decrease in polymer free volume.[45] The 400, 600, and 800 nm thick PMMA/Pd NP/SLG hybrid sensors upon exposure to 2% CO showed no gas response owing to successful sealing with PMMA layers as shown in Figure S3b in the Supporting Information. On the basis of this result, a 400 nm thick PMMA membrane was chosen as an optimal thickness for the PMMA layer to effectively act as a selectively H_2 permeable membrane.

Figure 5b shows the relative resistance changes of the Pd NP/SLG hybrid sensor without the PMMA membrane layer that was operated in an on−off mode for all gases: 1.4% gas response sensitivity for 10% CH_4, −2.08% gas response sensitivity for 0.5% CO, −5.17% gas response sensitivity for 0.05% NO_2, and 4.11% gas response sensitivity for 0.025% H_2. On the basis of these results, we concluded that the Pd NP/SLG hybrid sensor exhibited cross-sensitivity to all of the gases in the absence of the PMMA membrane layer, which could degrade the reliability and sensitivity of the sensor in gas mixtures. On the contrary, the PMMA membrane-coated Pd NP/SLG hybrid sensor did not exhibit a response upon exposure to 10% CH_4, 0.5% CO, and 0.05% NO_2 as shown in Figure 5c. To investigate the effect of other gases to the H_2 sensitivity, the PMMA membrane-coated Pd NP/SLG hybrid sensor was tested with flowing mixture gas of 0.025% H_2 and 0.05% NO_2 concurrently. First, the sensor was exposed to 0.025% H_2 and showed good operation in an on−off manner with a gas response sensitivity of ∼4% (blue solid line in Figure 5c), which is the similar value shown in Figure 4b and Figure 5b. When the sensor was then exposed to the mixture gas of 0.025% H_2 and 0.05% NO_2, the gas response sensitivity exhibited ∼4%, the value of which was attained upon exposure to 0.025% H_2 in previous experiment. This result implies that H_2 sensing is not affected in the presence of other gases because the PMMA membrane layer effectively blocks the other gases and selectively penetrate H_2. The selective filtration ability of the PMMA membrane layer was related to the free volume present in the PMMA polymer matrix.[45−48] Because the kinetic diameter of the H_2 molecules (0.289 nm) is smaller than that of NO_2 (0.4 nm), CO (0.33 nm), and CH_4 (0.38 nm), H_2 is more likely to penetrate the PMMA membrane layer than other gases. In fact, a higher permeability of H_2 in PMMA has been reported in numerous applications.[9,49] Our results showed that the PMMA membrane layer effectively functioned as a H_2 selective barrier without detriment to H_2 sensing property, which is significant in terms of safety, reliability, and sensitivity in dealing with H_2 sensors.

4. CONCLUSIONS

In summary, we demonstrated a PMMA/Pd NP/SLG hybrid sensor using a galvanic displacement reaction between graphene-buffered Cu and Pd ions, followed by spin-coating with a PMMA membrane layer to achieve high sensitivity and selectivity toward H_2. The fabricated sensor was tested with 0.025% H_2 as well as 10% CH_4, 0.5% CO, and 0.05% NO_2 with and without the PMMA membrane layer in order to investigate cross-sensitivity toward several gases. The PMMA/Pd NP/SLG hybrid sensor exhibited comparable and superior sensing performance upon exposure to H_2 compared to conventional graphene-Pd NP hybrid sensors. In addition, we observed that the PMMA/Pd NP/SLG hybrid sensor had good selectivity for H_2, showing no response upon exposure to CH_4, CO, or NO_2. The selective sensing of H_2 was attributed to the PMMA

DOI: 10.1021/am5073645
ACS Appl. Mater. Interfaces 2015, 7, 3554−3561

membrane layer, which was able to separate one or more gases from the gas mixture to facilitate a H_2-rich permeate. The highly sensitive sensor with gas selectivity toward H_2 reported herein meets the requirements of a good gas sensor, namely, no cross-sensitivity issues and excellent sensing performance for safety and reliable operation in gas mixtures.

■ ASSOCIATED CONTENT

Supporting Information

Additional figures (PDF). This material is available free of charge via the Internet at http://pubs.acs.org.

■ AUTHOR INFORMATION

Corresponding Author

*E-mail: taeyoon.lee@yonsei.ac.kr. Tel: +82-2-2123-5767. Fax: +82-2-313-2879.

Notes

The authors declare no competing financial interest.

■ ACKNOWLEDGMENTS

This work was supported by the Priority Research Centers Program through the National Research Foundation of Korea (NRF) funded by the Ministry of Education, Science and Technology (2012-0006689) and by the Industrial strategic technology development program (10041041, Development of nonvacuum and nonlithography based 5μm width Cu interconnect technology for TFT backplane) funded by the Ministry of Knowledge Economy (MKE, Korea). In addition, the authors would like to acknowledge the support of the Ministry of Higher Education, Kingdom of Saudi Arabia for supporting this research through a grant (PCSED-009-14) under the Promising Centre for Sensors and Electronic Devices (PCSED) at Najran University, Kingdom of Saudi Arabia. We thank the Tanaka Kikinzoku Kogyo K.K. for comments on the usage of palladium.

■ REFERENCES

(1) Goltsov, V. A.; Veziroglu, T. N. A step on the road to Hydrogen Civilization. *Int. J. Hydrogen Energy* **2002**, *27* (7−8), 719−723.

(2) Agbossou, K.; Chahine, R.; Hamelin, J.; Laurencelle, F.; Anouar, A.; St-Arnaud, J. M.; Bose, T. K. Renewable energy systems based on hydrogen for remote applications. *J. Power Sources* **2001**, *96* (1), 168−172.

(3) Buttner, W. J.; Post, M. B.; Burgess, R.; Rivkin, C. An overview of hydrogen safety sensors and requirements. *Int. J. Hydrogen Energy* **2011**, *36*, 2462−2470.

(4) Karim, G. A. Hydrogen as a spark ignition engine fuel. *Int. J. Hydrogen Energy* **2003**, *28*, 569−577.

(5) Firth, J. G.; Jones, A.; Jones, T. A. The principles of the detection of flammable atmospheres by catalytic devices. *Combust. Flame* **1973**, *20*, 303−311.

(6) Rahimi, F.; zad, A. I. Characterization of Pd nanoparticle dispersed over porous silicon as a hydrogen sensor. *J. Phys. D: Appl. Phys.* **2007**, *40*, 7201.

(7) Hübert, T.; Boon-Brett, L.; Black, G.; Banach, U. Hydrogen sensors − A review. *Sens. Actuators, B* **2011**, *157*, 329−352.

(8) Salomonsson, A.; Eriksson, M.; Dannetun, H. Hydrogen interaction with platinum and palladium metal−insulator−semiconductor devices. *J. Appl. Phys.* **2005**, *98*, 014505−014505−10.

(9) Jang, B.; Lee, K. Y.; Noh, J.-S.; Lee, W. Nanogap-based electrical hydrogen sensors fabricated from Pd-PMMA hybrid thin films. *Sens. Actuators, B* **2014**, *193*, 530−535.

(10) Walter, E. C.; Favier, F.; Penner, R. M. Palladium Mesowire Arrays for Fast Hydrogen Sensors and Hydrogen-Actuated Switches. *Anal. Chem.* **2002**, *74*, 1546−1553.

(11) Mor, G. K.; Varghese, O. K.; Paulose, M.; Ong, K. G.; Grimes, C. A. Fabrication of hydrogen sensors with transparent titanium oxide nanotube-array thin films as sensing elements. *Thin Solid Films* **2006**, *496*, 42−48.

(12) Wan, J. K. S.; Ioffe, M. S.; Depew, M. C. A novel acoustic sensing system for on-line hydrogen measurements. *Sens. Actuators, B* **1996**, *32*, 233−237.

(13) Qurashi, A.; Yamazaki, T.; El-Maghraby, E. M.; Kikuta, T. Fabrication and gas sensing properties of In2O3 nanopushpins. *Appl. Phys. Lett.* **2009**, *95*, 153109−153109−3.

(14) Wang, B.; Zhu, L. F.; Yang, Y. H.; Xu, N. S.; Yang, G. W. Fabrication of a SnO2 Nanowire Gas Sensor and Sensor Performance for Hydrogen. *J. Phys. Chem. C* **2008**, *112*, 6643−6647.

(15) Junghwan, H.; Jonghyurk, P.; Gyu Tae, K.; Jeong Young, P. Highly sensitive hydrogen detection of catalyst-free ZnO nanorod networks suspended by lithography-assisted growth. *Nanotechnology* **2011**, *22*, 085502−085502−7.

(16) Jun, Y.-K.; Kim, H.-S.; Lee, J.-H.; Hong, S.-H. High H_2 sensing behavior of TiO2 films formed by thermal oxidation. *Sens. Actuators, B* **2005**, *107*, 264−270.

(17) Pak, Y.; Kim, S.-M.; Jeong, H.; Kang, C. G.; Park, J. S.; Song, H.; Lee, R.; Myoung, N.; Lee, B. H.; Seo, S.; Kim, J. T.; Jung, G.-Y. Palladium-Decorated Hydrogen-Gas Sensors Using Periodically Aligned Graphene Nanoribbons. *ACS Appl. Mater. Interfaces* **2014**, *6*, 13293−13298.

(18) Lu, G.; Miura, N.; Yamazoe, N. High-temperature hydrogen sensor based on stabilized zirconia and a metal oxide electrode. *Sens. Actuators, B* **1996**, *35*, 130−135.

(19) Goltsova, M. V.; Artemenko, Y. A.; Zaitsev, V. I. Kinetics and morphology of the reverse $\beta \rightarrow \alpha$ hydride transformation in thermodynamically open Pd−H system. *J. Alloys Compd.* **1999**, *293−295*, 379−384.

(20) Pundt, A. Hydrogen in Nano-sized Metals. *Adv. Eng. Mater.* **2004**, *6*, 11−21.

(21) Lee, J.; Shim, W.; Lee, E.; Noh, J.-S.; Lee, W. Highly Mobile Palladium Thin Films on an Elastomeric Substrate: Nanogap-Based Hydrogen Gas Sensors. *Angew. Chem.* **2011**, *123*, 5413−5417.

(22) Zeng, X. Q.; Latimer, M. L.; Xiao, Z. L.; Panuganti, S.; Welp, U.; Kwok, W. K.; Xu, T. Hydrogen Gas Sensing with Networks of Ultrasmall Palladium Nanowires Formed on Filtration Membranes. *Nano Lett.* **2010**, *11*, 262−268.

(23) Lee, J. M.; Park, J.-e.; Kim, S.; Kim, S.; Lee, E.; Kim, S.-J.; Lee, W. Ultra-sensitive hydrogen gas sensors based on Pd-decorated tin dioxide nanostructures: Room temperature operating sensors. *Int. J. Hydrogen Energy* **2010**, *35*, 12568−12573.

(24) Kolmakov, A.; Klenov, D. O.; Lilach, Y.; Stemmer, S.; Moskovits, M. Enhanced Gas Sensing by Individual SnO_2 Nanowires and Nanobelts Functionalized with Pd Catalyst Particles. *Nano Lett.* **2005**, *5*, 667−673.

(25) Catalano, J.; Giacinti Baschetti, M.; Sarti, G. C. Hydrogen permeation in palladium-based membranes in the presence of carbon monoxide. *J. Membr. Sci.* **2010**, *362*, 221−233.

(26) Jung, S. H.; Kusakabe, K.; Morooka, S.; Kim, S.-D. Effects of co-existing hydrocarbons on hydrogen permeation through a palladium membrane. *J. Membr. Sci.* **2000**, *170*, 53−60.

(27) Dan, Y.; Lu, Y.; Kybert, N. J.; Luo, Z.; Johnson, A. T. C. Intrinsic Response of Graphene Vapor Sensors. *Nano Lett.* **2009**, *9*, 1472−1475.

(28) Schedin, F.; Geim, A. K.; Morozov, S. V.; Hill, E. W.; Blake, P.; Katsnelson, M. I.; Novoselov, K. S. Detection of individual gas molecules adsorbed on graphene. *Nat. Mater.* **2007**, *6*, 652−655.

(29) Huang, B.; Li, Z.; Liu, Z.; Zhou, G.; Hao, S.; Wu, J.; Gu, B.-L.; Duan, W. Adsorption of Gas Molecules on Graphene Nanoribbons and Its Implication for Nanoscale Molecule Sensor. *J. Phys. Chem. C* **2008**, *112*, 13442−13446.

(30) Fowler, J. D.; Allen, M. J.; Tung, V. C.; Yang, Y.; Kaner, R. B.; Weiller, B. H. Practical Chemical Sensors from Chemically Derived Graphene. *ACS Nano* **2009**, *3*, 301−306.

DOI: 10.1021/am5073645
ACS Appl. Mater. Interfaces 2015, 7, 3554−3561

(31) Geim, A. K.; Novoselov, K. S. The rise of graphene. *Nat. Mater.* **2007**, *6*, 183−191.
(32) Johnson, J. L.; Behnam, A.; Pearton, S. J.; Ural, A. Hydrogen Sensing Using Pd-Functionalized Multi-Layer Graphene Nanoribbon Networks. *Adv. Mater.* **2010**, *22*, 4877−4880.
(33) Wu, W.; Liu, Z.; Jauregui, L. A.; Yu, Q.; Pillai, R.; Cao, H.; Bao, J.; Chen, Y. P.; Pei, S.-S. Wafer-scale synthesis of graphene by chemical vapor deposition and its application in hydrogen sensing. *Sens. Actuators, B* **2010**, *150*, 296−300.
(34) Chung, M. G.; Kim, D.-H.; Seo, D. K.; Kim, T.; Im, H. U.; Lee, H. M.; Yoo, J.-B.; Hong, S.-H.; Kang, T. J.; Kim, Y. H. Flexible hydrogen sensors using graphene with palladium nanoparticle decoration. *Sens. Actuators, B* **2012**, *169*, 387−392.
(35) Phan, D.-T.; Chung, G.-S. Characteristics of resistivity-type hydrogen sensing based on palladium-graphene nanocomposites. *Int. J. Hydrogen Energy* **2014**, *39*, 620−629.
(36) Wang, H.; Wang, G.; Bao, P.; Yang, S.; Zhu, W.; Xie, X.; Zhang, W.-J. Controllable Synthesis of Submillimeter Single-Crystal Monolayer Graphene Domains on Copper Foils by Suppressing Nucleation. *J. Am. Chem. Soc.* **2012**, *134*, 3627−3630.
(37) Hong, J.; Lee, S.; Lee, S.; Han, H.; Mahata, C.; Yeon, H.-W.; Koo, B.; Kim, S.-I.; Nam, T.; Byun, K.; Min, B.-W.; Kim, Y.-W.; Kim, H.; Joo, Y.-C.; Lee, T. Graphene as an atomically thin barrier to Cu diffusion into Si. *Nanoscale* **2014**, *6*, 7503−7511.
(38) Wang, S.; Lin, W.; Zhu, Y.; Xie, Y.; McCormick, J.; Huang, W.; Chen, J. Pd-based bimetallic catalysts prepared by replacement reactions. *Catal. Lett.* **2007**, *114*, 169−173.
(39) Zhao, H.; Yang, J.; Wang, L.; Tian, C.; Jiang, B.; Fu, H. Fabrication of a palladium nanoparticle/graphene nanosheet hybrid via sacrifice of a copper template and its application in catalytic oxidation of formic acid. *Chem. Commun.* **2011**, *47*, 2014−2016.
(40) Graf, D.; Molitor, F.; Ensslin, K.; Stampfer, C.; Jungen, A.; Hierold, C.; Wirtz, L. Spatially Resolved Raman Spectroscopy of Single- and Few-Layer Graphene. *Nano Lett.* **2007**, *7*, 238−242.
(41) Seo, J.; Lee, S.; Han, H.; Jung, H. B.; Hong, J.; Song, G.; Cho, S. M.; Park, C.; Lee, W.; Lee, T. Gas-Driven Ultrafast Reversible Switching of Super-hydrophobic Adhesion on Palladium-Coated Silicon Nanowires. *Adv. Mater.* **2013**, *25*, 4139−4144.
(42) Lewis, F. A. Palladium hydrogen system. *Platinum Met. Rev.* **1982**, *26*, 20−27.
(43) Xu, T.; Zach, M. P.; Xiao, Z. L.; Rosenmann, D.; Welp, U.; Kwok, W. K.; Crabtree, G. W. Self-assembled monolayer-enhanced hydrogen sensing with ultrathin palladium films. *Appl. Phys. Lett.* **2005**, *86*, 203104−203104−3.
(44) Uemiya, S.; Kato, W.; Uyama, A.; Kajiwara, M.; Kojima, T.; Kikuchi, E. Separation of hydrogen from gas mixtures using supported platinum-group metal membranes. *Sep. Purif. Technol.* **2001**, *22*−*23*, 309−317.
(45) Acharya, N. K.; Kulshrestha, V.; Awasthi, K.; Jain, A. K.; Singh, M.; Vijay, Y. K. Hydrogen separation in doped and blend polymer membranes. *Int. J. Hydrogen Energy* **2008**, *33*, 327−331.
(46) Kumar, S.; Sharma, A.; Tripathi, B.; Srivastava, S.; Agrawal, S.; Singh, M.; Awasthi, K.; Vijay, Y. K. Enhancement of hydrogen gas permeability in electrically aligned MWCNT-PMMA composite membranes. *Micron* **2010**, *41*, 909−914.
(47) Tung, K.-L.; Lu, K.-T. Effect of tacticity of PMMA on gas transport through membranes: MD and MC simulation studies. *J. Membr. Sci.* **2006**, *272*, 37−49.
(48) Hosseini, S. S.; Teoh, M. M.; Chung, T. S. Hydrogen separation and purification in membranes of miscible polymer blends with interpenetration networks. *Polymer* **2008**, *49*, 1594−1603.
(49) Jeon, K.-J.; Moon, H. R.; Ruminski, A. M.; Jiang, B.; Kisielowski, C.; Bardhan, R.; Urban, J. J. Air-stable magnesium nanocomposites provide rapid and high-capacity hydrogen storage without using heavy-metal catalysts. *Nat. Mater.* **2011**, *10*, 286−290.

DOI: 10.1021/am5073645
ACS Appl. Mater. Interfaces 2015, 7, 3554−3561